HEAVY ION FUSION SCIENCE VIRTUAL NATIONAL
LABORATORY
1ST QUARTER 2010
MILESTONE REPORT
Simulations of fast correction of chromatic aberrations to
establish physics specifications for implementation on
NDCX-1 and NDCX-2

by
S.M. LUND LLNL, Livermore, CA 94550 USA
S.M. LIDIA, P.A. SEIDL LBNL, Berkeley, CA 94720, USA

Accelerator Fusion Research Division
Ernest Orlando Lawrence Berkeley National Laboratory
University of California
Berkeley, California 94720

January 2010

HEAVY ION FUSION SCIENCE VIRTUAL NATIONAL LABORATORY

1ST QUARTER 2010

MILESTONE REPORT

<div style="background-color:salmon">

Simulations of fast correction of chromatic aberrations to establish physics specifications for implementation on NDCX-1 and NDCX-2.

</div>

S.M. LIDIA*, S.M. LUND** and P.A. SEIDL*

*Lawrence Berkeley National Laboratory
**Lawrence Livermore National Laboratory

1. SUMMARY

This milestone has been accomplished. The Heavy Ion Fusion Science Virtual National Laboratory has completed simulations of a fast correction scheme to compensate for chromatic and time-dependent defocusing effects in the transport of ion beams to the target plane in the NDCX-1 facility. Physics specifications for implementation in NDCX-1 and NDCX-2 have been established.

2. Executive Summary

This milestone has been accomplished. The Heavy Ion Fusion Science Virtual National Laboratory has completed simulations of a fast correction scheme to compensate for chromatic and time-dependent defocusing effects in the transport of ion beams to the target plane in the NDCX-1 facility. Physics specifications for implementation in NDCX-1 and NDCX-2 have been established.

Focal spot differences at the target plane between the compressed and uncompressed regions of the beam pulse have been modeled and measured on NDCX-1. Time-dependent focusing and energy sweep from the induction bunching module are seen to increase the compressed pulse spot size at the target plane by factors of two or more, with corresponding scaled reduction in the peak intensity and fluence on target. A time-varying beam envelope correction lens has been suggested to remove the time-varying aberration.

An Einzel (axisymmetric electric) lens system has been analyzed and optimized for general transport lines, and as a candidate correction element for NDCX-1. Attainable high-voltage holdoff and temporal variations of the lens driving waveform are seen to effect significant changes on the beam envelope angle over the duration of interest, thus confirming the utility of such an element on NDCX-1.
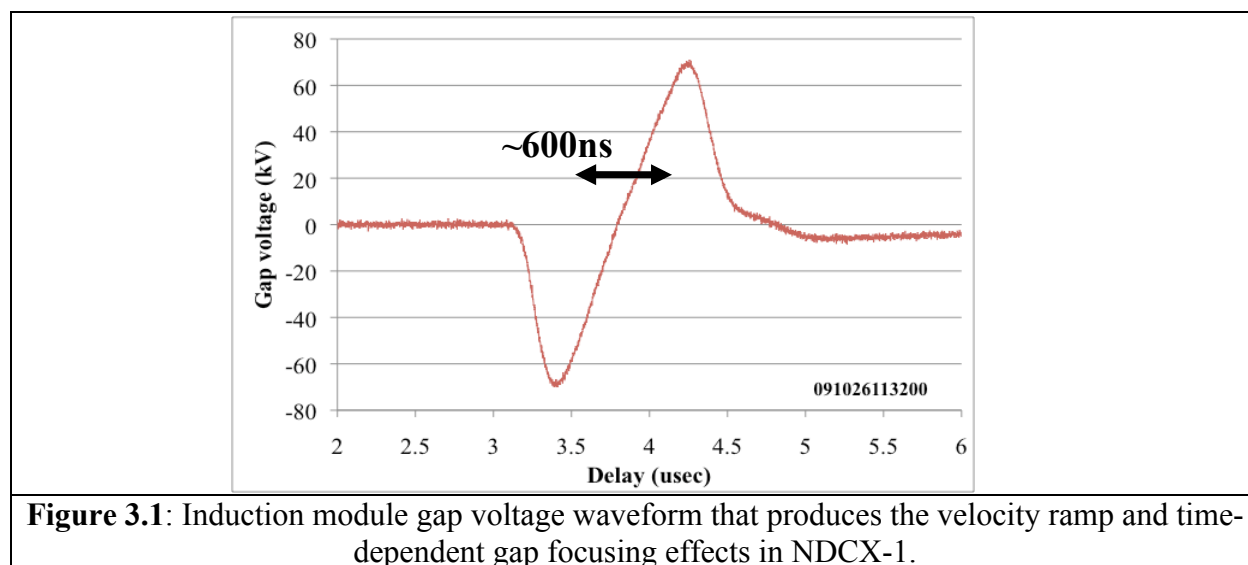
Modeling of the beam dynamics in NDCX-1 was performed using a time-dependent (slice) envelope code and with the 3-D, self-consistent, particle-in-cell code WARP. Proof of concept was established with the slice envelope model such that the spread in beam waist positions relative to the target plane can be minimized with a carefully designed Einzel lens waveform and transport line. WARP simulations have verified the efficacy of the Einzel lens while including more detailed beam physics. WARP simulations have also indicated some unpredicted transit-time effects, and methods are currently being explored to compensate and reduce this complication.

We have explored the use of an Einzel lens, or system of Einzel lenses, to compensate for chromatic aberrations in the beam focal spot in the NDCX-2 target plane. The final beam manipulations in NDCX-2 (linear velocity ramp, charge neutralization, high field final focus solenoid) are similar to NDCX-1 though the NDCX-2 beam has much higher energy and current. The most relevant distinctions are that the pulse duration at the entrance to the drift compression section is tenfold shorter, and that the beam energy tenfold higher, than in NDCX-1. Placing a time-dependent, envelope angle correcting element at the neutralized drift region entrance presents a very significant challenge to voltage holdoff and voltage swing V(t) in a single Einzel lens. Placing the Einzel lens(es) further upstream reduces the required voltage risetime V'(t) to effect the necessary envelope correction, while increasing the duration over which the time-dependent voltage must vary. While this simplifies the technological challenge of designing and operating a Einzel lens in NDCX-2, it does require much finer control of the correcting waveform and measurements of its effect on space-charge dominated beams over a much longer axial path length to target than in the NDCX-1.
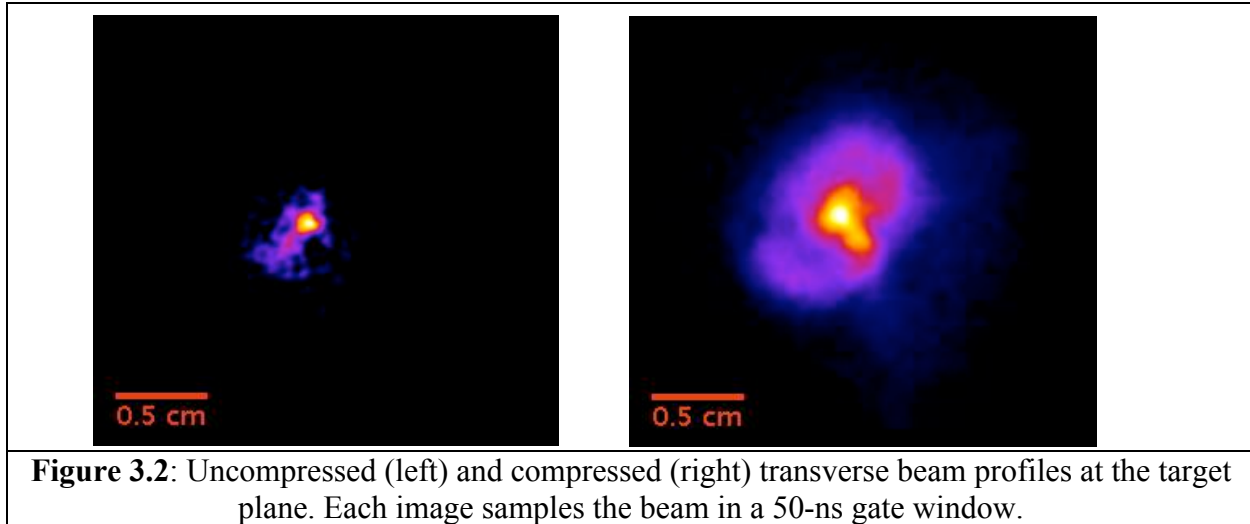
3. Introduction

NDCX-1 has demonstrated the effectiveness of longitudinal compression of a drifting neutralization beam by a large (~15%) head-to-tail velocity ramp. This ramp is produced by a rising electric potential across a beam-line gap, induced by a specially programmed induction module. Unwanted, time-dependent dynamical effects accompany the imposition of the ramp: ion trajectory angles are reduced in proportion to gap entry angle and added velocity; there is a transverse focusing effect from the axisymmetric lens produced along with the accelerating field; and the finite transit time across the acceleration gap performs a time window-averaging of the modulation. These produce an average defocusing change of 5-6 mrad in the ~20 mrad envelope angle of convergence. This time-dependent angle and energy variation in turn causes the longitudinal focal position to sweep by about 10% (of the final focusing solenoid focal length) from the intended spot, causing a large reduction in the bunched beam intensity on target. Hence, it is desired to correct the time-dependent focal plane of the strong final focus lens (~8 Tesla). The problem is an intrinsic one for neutralized compression and solutions are sought for NDCX-1, NDCX-2 and heavy-ion fusion drivers.
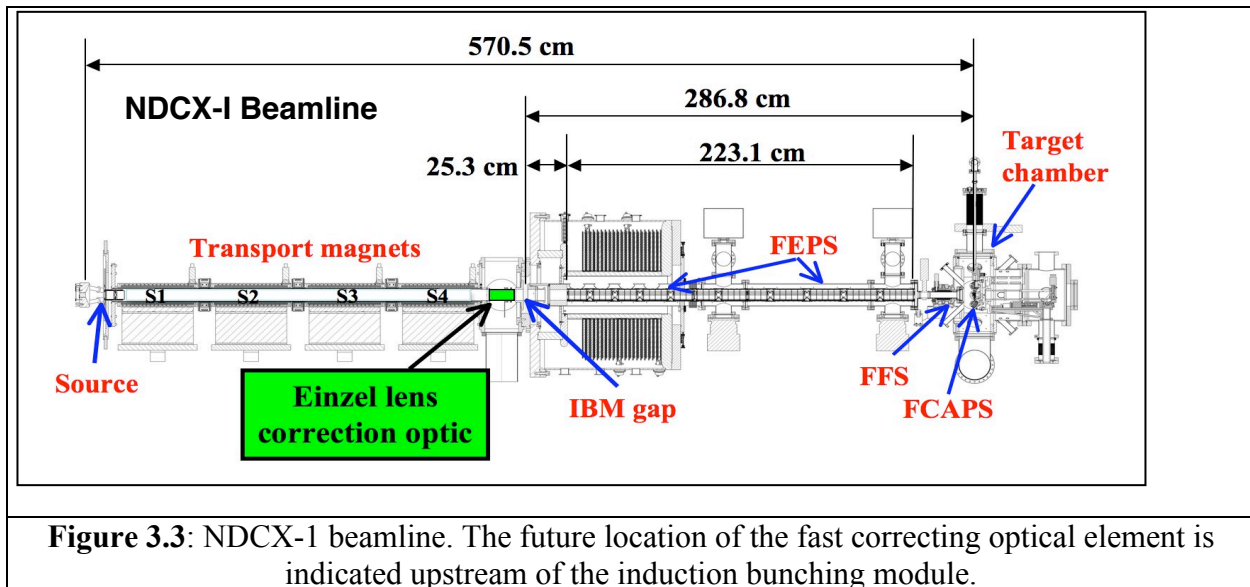
The time-dependent transverse focusing effect has been observed in recent NDCX-1 beam measurements. Fig 3.1 shows an example of the bipolar voltage waveform from the induction bunching module (IBM) that impresses a velocity ramp on the beam.

Figure 3.1: Induction module gap voltage waveform that produces the velocity ramp and time-dependent gap focusing effects in NDCX-1.

The earlier and later portions of the 5-15 μs beam pulse are left un-modulated by the IBM gap voltage waveform, and are delivered to the target region without longitudinal pulse compression. These uncompressed regions maintain the average beam current and kinetic energy as they are focused unto the target plane. The transverse beam profiles for the uncompressed and compressed regions of the beam are shown in Fig. 3.2. The time-dependent and chromatic effects on the final focus optics are clearly evident in the increased spot size of the modulated beam and the large, diffuse beam halo. The spot size (as measured by the 50% intensity diameter) increases from ~1.5 mm in the uncompressed region to >3 mm in the compressed portion of the beam pulse.

Figure 3.2: Uncompressed (left) and compressed (right) transverse beam profiles at the target plane. Each image samples the beam in a 50-ns gate window.

To correct this effect, an additional time-dependent impulse to the beam envelope can be imposed either following or preceding the IBM. This angle correction can be programmed in such a way that the unwanted dynamical effect of the IBM is cancelled at the target plane. In the NDCX-1 case, this correction requires that a rapidly pulsed lens add ~10 mrad to the envelope during the ~500 ns time of passage through the lens. The pulsed lens should be as short as practical to minimize the transit time effects and space-charge defocusing of the beam, and it should operate in vacuum close to the bunching module. The NDCX-1 beamline is shown in Fig. 3.3.

Figure 3.3: NDCX-1 beamline. The future location of the fast correcting optical element is indicated upstream of the induction bunching module.
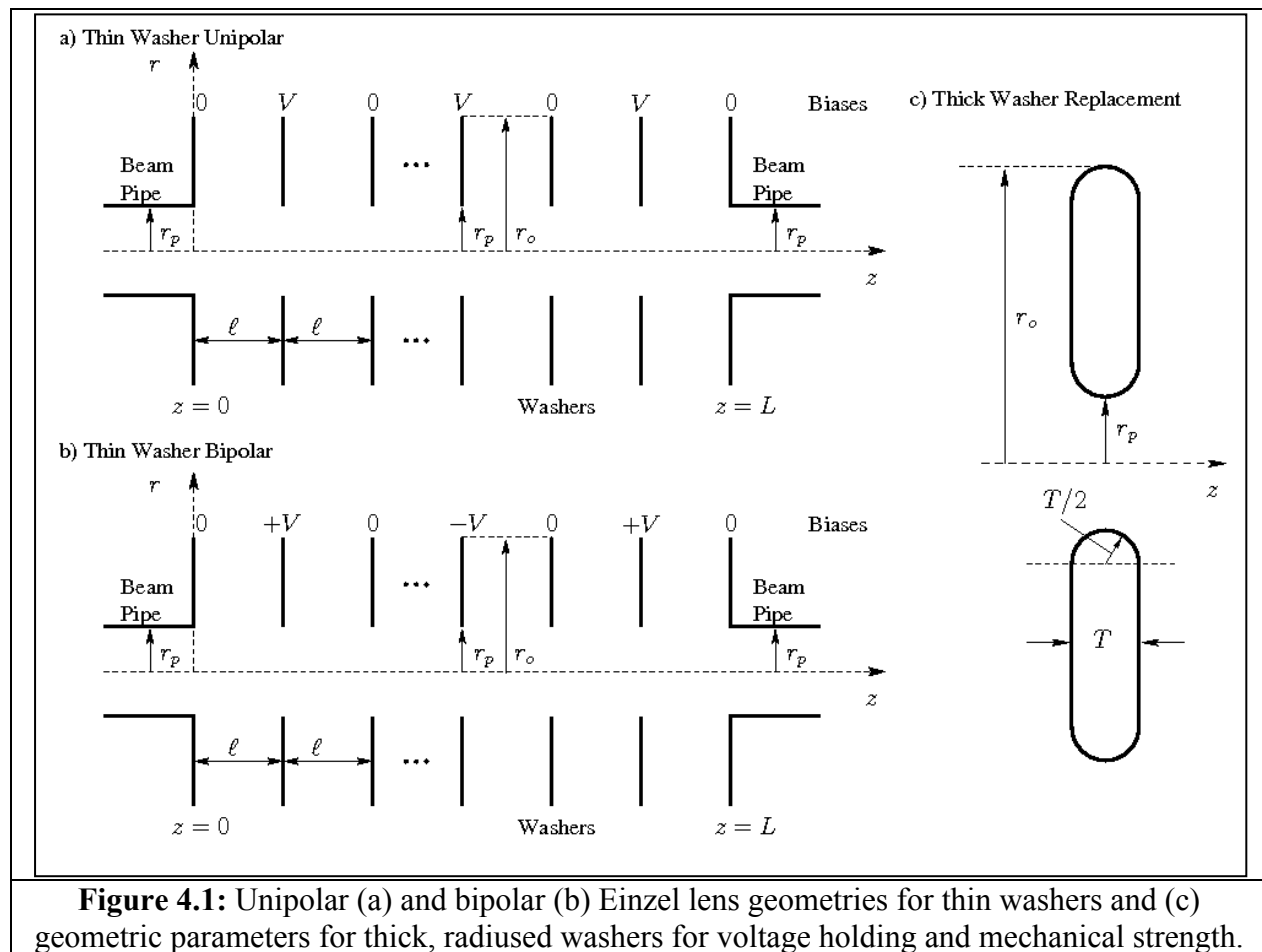
A first look at requirements for such a pulsed lens indicates that a pulsed electric Einzel lens or quadrupole doublet with modest potentials can meet the requirements. This is a low cost application of a well-known technology. Alternatively, a quadrupole triplet would allow correction of non-axisymmetric *rms*-envelope parameters at injection to the bunching module to be brought to an axisymmetric distribution at the focal plane. This would increase the overall

length of the correction element and will be studied in further simulations. In spite of weaker focusing strength, axisymmetric Einzel lens configurations are considered more desirable relative to quadrupole optics because they are most easily integrated into the ideally axisymmetric solenoid transport line. It is possible that a single correction element would be difficult to tune due to sensitivities to the evolving beam parameters and possible particle loss in the relatively small-diameter final focus magnet beam pipe. Therefore a second time dependent correction element, separated longitudinally from the first might be preferred. These sensitivities and design issues are being explored using envelope models and PIC simulations.

4. Einzel Lens Design and Optimization

Numerous configurations of Einzel lens optics are possible. A "stacked washer" configuration illustrated in Fig. 4.1 was selected due to attractive voltage holding characteristics and ease in fabrication. Plates can be biased in both unipolar and bipolar configurations as indicated. Einzel lenses are *always focusing* irrespective of the bias polarity. This constrains requirements for tuning in the machine lattice (see Sec. 5).

Figure 4.1: Unipolar (a) and bipolar (b) Einzel lens geometries for thin washers and (c) geometric parameters for thick, radiused washers for voltage holding and mechanical strength.

An extensive study on the focusing properties of stacked washer Einzel lenses provided an

understanding of optimal geometric properties to enhance focusing strength and decrease nonlinear aberrations for a given aspect ratio. This study is broadly applicable in accelerator applications beyond those considered here and will be submitted for publication in 2010. A reduced dynamical model for the linear focusing properties of general Einzel lens systems has been derived together with a corresponding envelope model for analysis of transport of beams with strong space-charge. In this formulation the Einzel lens systems are described by their on-axis potential variation. Accurate analytical models for the potential of stacked washer Einzel lens systems with thin washers were derived and this model was applied to show that the linear focusing strength is optimized for unipolar and bipolar system for ratios of aperture (r_p) to washer spacing (l) of $r_p/l \approx 0.4688$ for unipolar systems and $r_p/l \approx 0.9377$ for bipolar systems. Fig. 4.2 shows the effective focusing strength for unipolar and bipolar systems plotted as a function of aspect ratio r_p/l for several values of bias potential to particle kinetic energy (qV/E_b). Dashed vertical lines correspond to the optimal values of r_p/l for maximum focusing strength (marked with dots on curves), which shift only very weakly as a function of qV/E_b. Note that for the same bias strength (i.e., value of qV/E_b), bipolar systems have considerably stronger focusing strength (~3 times unipolar strength) at optimal aspect ratio values and have less sensitivity to the optimal aspect ratio.
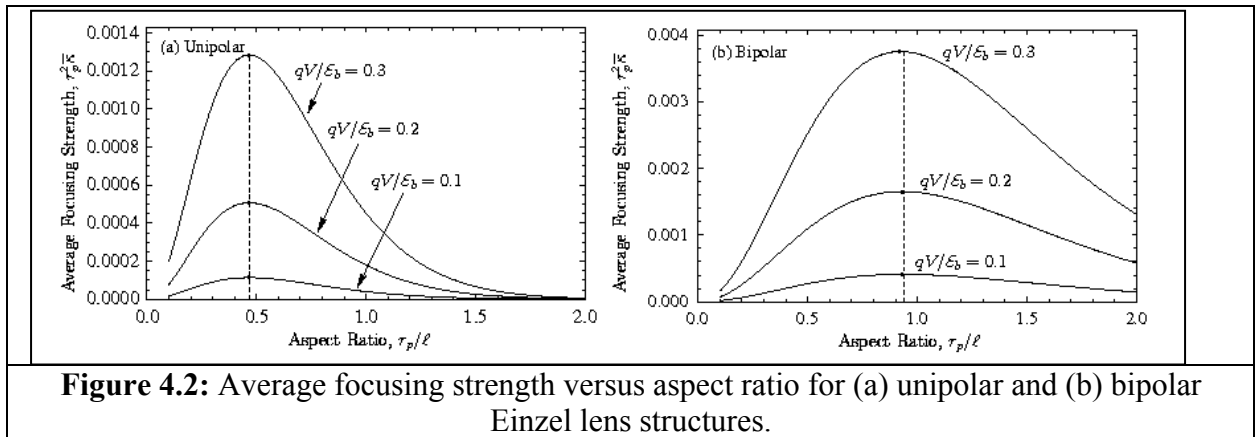
Figure 4.2: Average focusing strength versus aspect ratio for (a) unipolar and (b) bipolar Einzel lens structures.

It is desirable to minimize radial washer extent (r_o) to control system radial build and biased washers edges must have finite thickness for mechanical strength and to allow use of radiused (rounded) edges to limit break-down inducing peak field strengths. Studies indicate that the washers can be terminated at $r_o \geq 2.5 \, r_p$ with negligible deficit in focusing strength.

The effect of finite washer thickness was studied using numerical field solutions in the WARP code (see Sec. 5.2) and it was found that increased washer thickness results in stronger linear focusing strength. However, in spite of this washer thickness is kept minimally sufficient to hold peak fields safely below breakdown values which scale as $100(kV/cm)\sqrt{(1cm/l)}$ because gains in focusing strength with modest increases in washer thickness are minimal. Addition motivation for thin washers is that increased biased washer thickness can lead to greater chances that particles will be lost at grazing incidence, which can initiate electrical discharges and breakdown. The high particle flux and complicated beam manipulations in the NDCX machines make such lost particle induced failures in voltage holding an issue of concern.
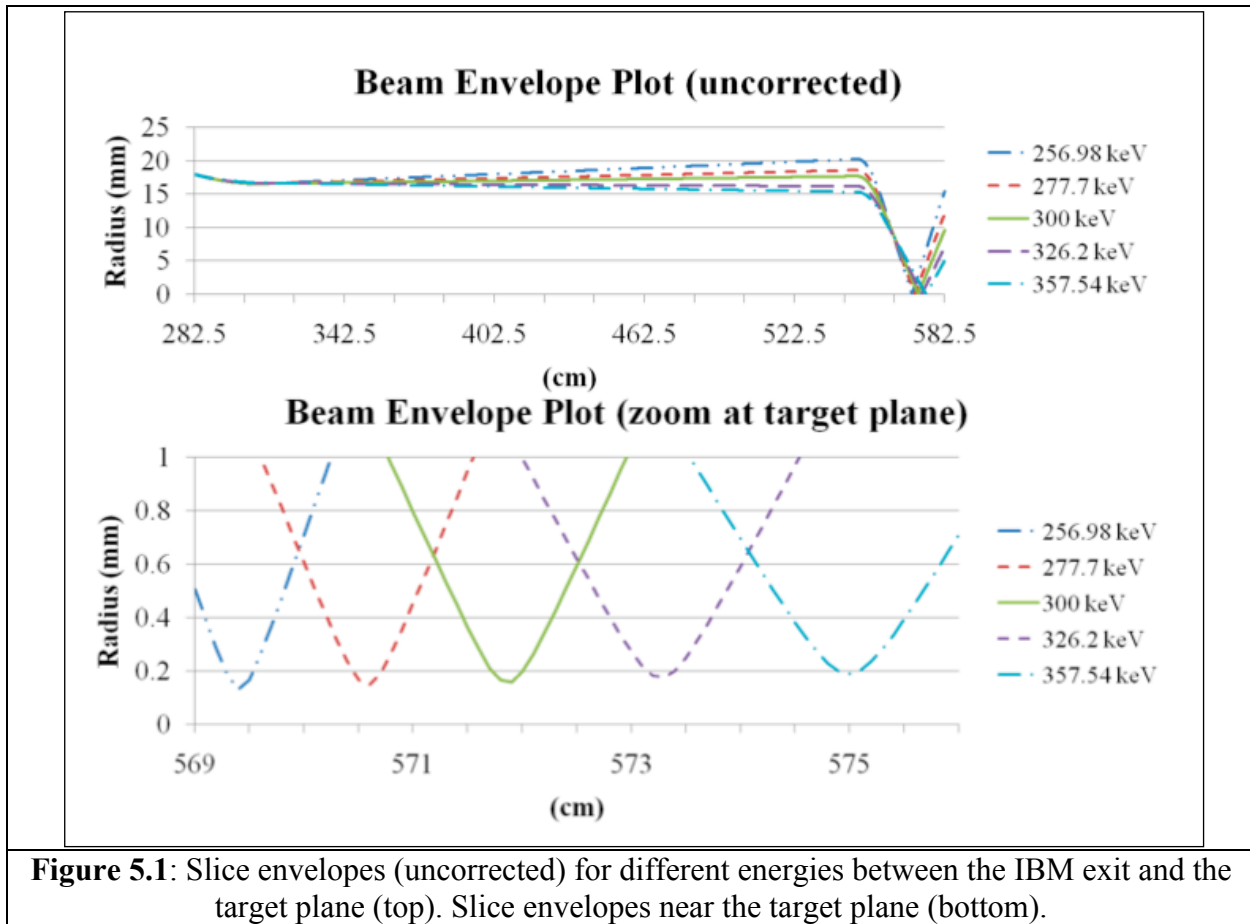
5. Modeling Performance and Simulations for NDCX-1

We have modeled the beam physics and performance of an Einzel lens fast correcting element by various analytical and numerical models. A simple multi-slice, multi-energy envelope code was constructed to enable quick studies of parameter dependence and optimization. The WARP particle-in-cell (PIC) code has been configured to handle unipolar or bipolar Einzel lens systems with varying geometry and driving potential waveforms. WARP simulations will allow evaluation of system performance at a high level of detail.

5.1 Slice Envelope Solver

A numerical slice envelope equation solver was implemented in MatLab[i] to calculate the radial and temporal evolution of individual slices carrying varying charge and energy. The slice tracking begins at the entrance to the IBM and follows the slices to the target plane. In this model, the IBM gap is assumed to be accurately described as a thin lens, while the fringe fields of the 8 Tesla final focus solenoid are included. Except for a ~25cm length following the IBM gap, the rest of the ~287cm drift length is assumed to be uniformly filled with a completely charge-neutralizing plasma. The Einzel lens is modeled by an analytical potential model that takes into account the fringe entering and exiting the optic

The uncorrected envelopes for the range of slice energies are shown in Fig. 5.1. This ensemble represents a magnetic lattice tune that optimizes the beam fluence at the target plane, but does not yet correct for chromatic aberrations. Each slice reaches an emittance-limited spot size at its waist.

Figure 5.1: Slice envelopes (uncorrected) for different energies between the IBM exit and the target plane (top). Slice envelopes near the target plane (bottom).

The beamline coordinates and initial beam envelope conditions are given in Tables 5.1 and 5.2.

Table 5.1: Initial beam conditions.

|	
Center energy	300 keV
Initial current	27 mA
Initial pulse duration	400 ns
Longitudinal beam temperature	1 eV
Normalized transverse emittance	0.06π mm-mrad
Target plane distance from source	570.5 cm
FFS peak field	7.4 Tesla
Beam pipe aperture radius	20 mm

Table 5.2: Initial envelope parameters.

Plane	z (cm)	a (mm)	a' (mrad)
'Box 1'	262.5	21.4	-13.5
IBM entrance	282.5	18	-13.5
IBM exit	282.5	18	-10.5

From Fig. 5.1 it is readily seen that there is a considerable spread in focal planes for slices of varying energies. Hence a target placed at any one location will intercept a narrow range of energies at the slice waists, but that off-energy slices will have much larger radii. The peak beam fluence suffers accordingly.

A prescriptive, correlated correction to the envelope convergence angle as it exits the IBM has been empirically found to improve the beam fluence at the target plane. The correction is shown in Fig. 5.2. An iterative search procedure re-optimizes the initial envelope parameters so that an additional correlated correction to the envelope angle places the slice envelope waists nearer to the target plane.

Figure 5.2: Correlated envelope angle correction and IBM voltage.
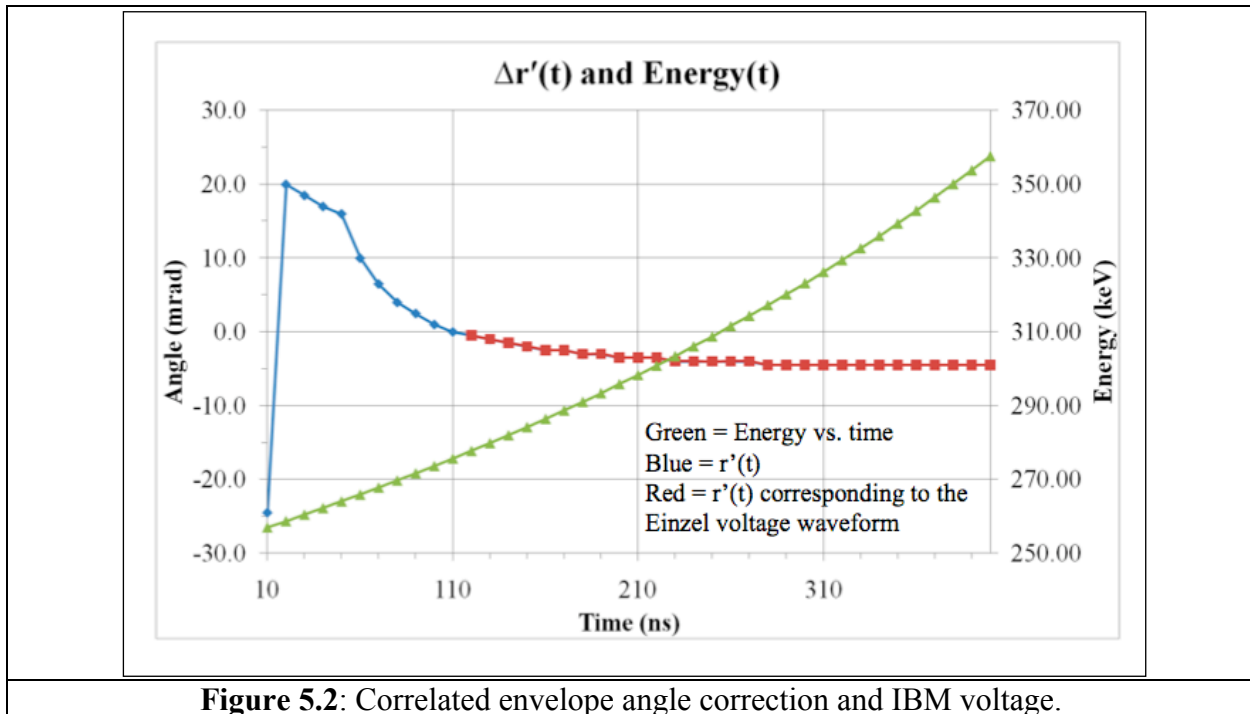
The corrected envelopes are shown in Fig. 5.3. The lowest energy slice (~257 keV) is shown to scrape and is presumed lost. The beam aperture (20 mm radius) just upstream from the target chamber limits transmission of the beam spectrum up to ~270 keV. This is partly a function of the initial conditions upstream of the IBM and neutralization channel, and the available range of beam envelope parameters doesn't permit correction of the full energy range.

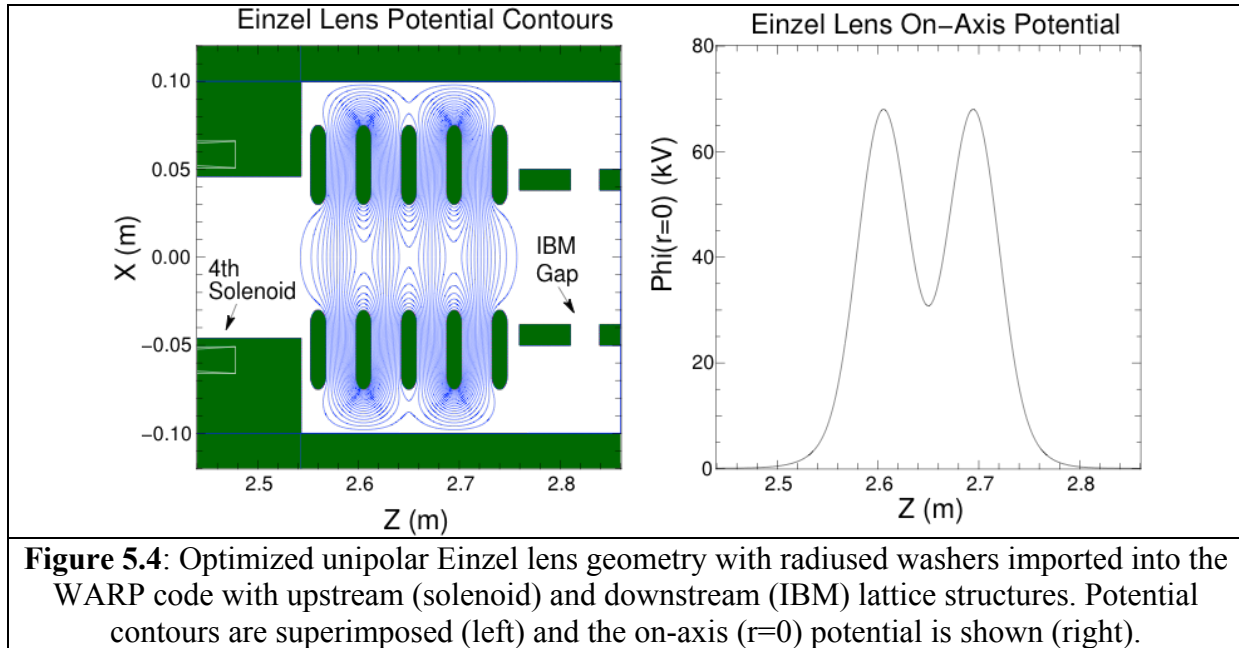**Figure 5.3**: Corrected slice envelopes over the drift length (top) and near the target plane (bottom).
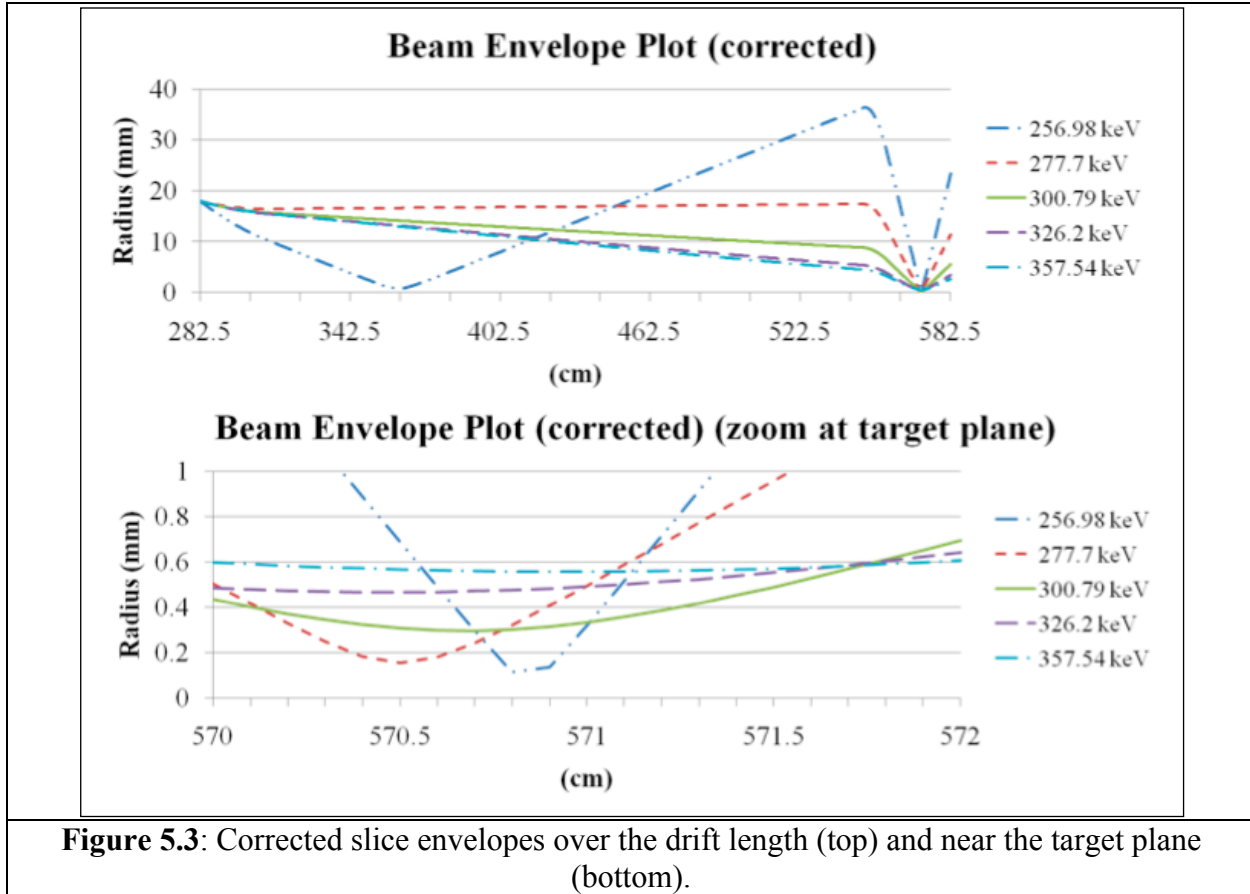
Comparing the two optimized tunes (Fig. 5.1 and Fig. 5.3), the correction works by increasing the waist size and the Rayleigh range of the slices over the specified energy range. The overlap of the slice envelopes at the target plane is dramatically increased.

5.2 WARP Modeling

Extensive 3D and *r-z* simulations of the NDCX-1 beam dynamics have been carried out with the WARP PIC code. These simulations include the full detailed geometry of the lattice, a thick-coil solenoid magnet model with eddy current corrections, waveforms for the Marx and IBM pulsers imported from experimentally measured data, and an extensive hierarchy of static and kinetic neutralizing plasma models. Although these simulations have not been accurate to date in terms of precise quantitative predictions of the beam fluence on target, they have been valuable in providing guidance on trends in the beam dynamics, tuning, optimization, and in interpreting experimental results. The WARP simulations are large and typically the full machine pulse cycle is simulated from the beam head emerging off the source to the late stages of the pulse impinging on the target. Full 3D runs can include lattice errors and other asymmetries and when using a full kinetic plasma mode can require days of computer time using all of the group's parallel computer resources. Reduced *r-z* simulations with a simple neutralized plasma model typically take 4 hours on a single processor and many parametric runs can be rapidly carried out (up to 3000 full machine cycle runs per day at usual resolutions) by distributing serial runs on individual
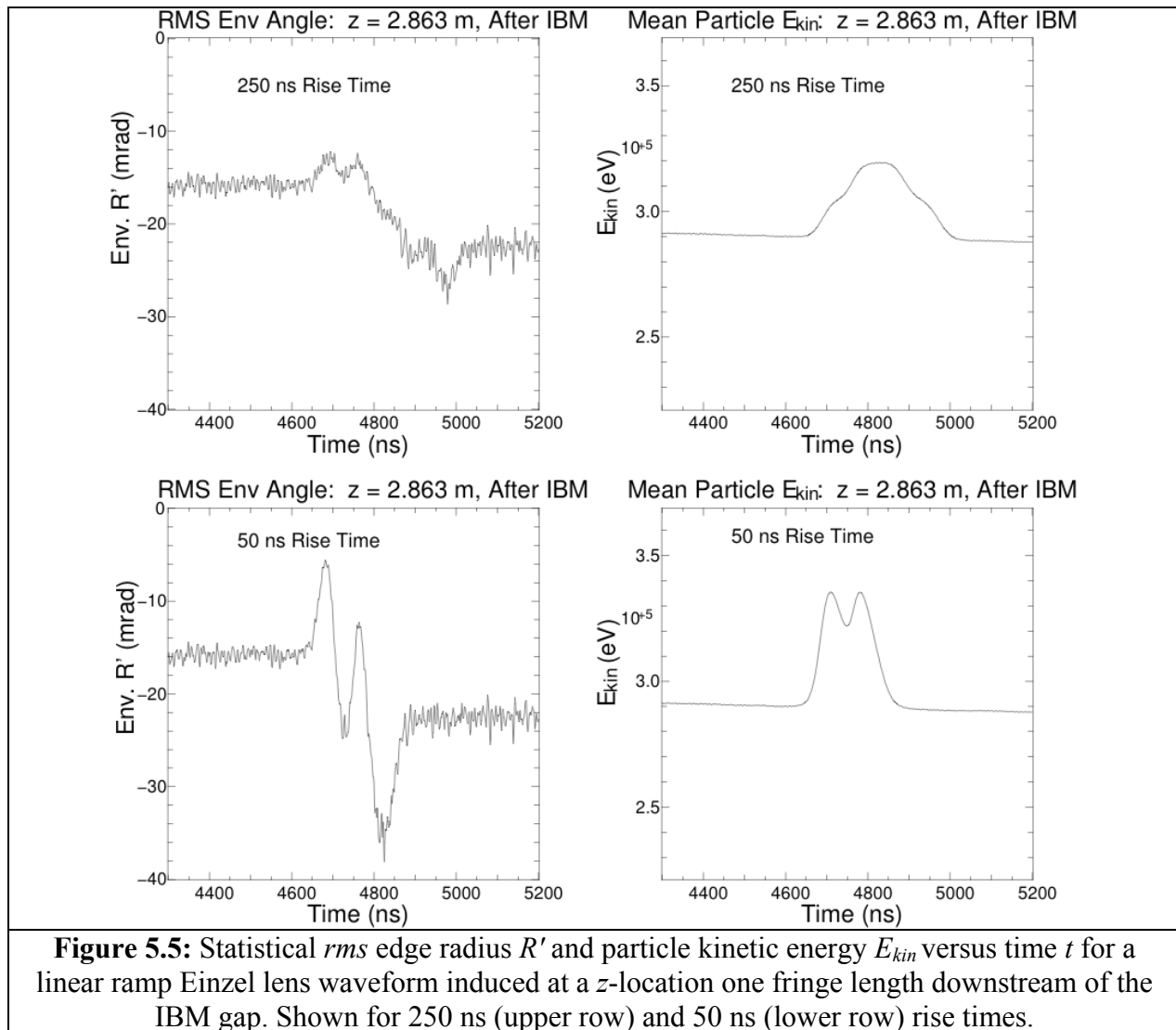
processors of the group computing cluster.

We successfully incorporated pulsed stacked-washer Einzel lens models into the WARP code structure while maintaining full functionality of all 3D and *r-z* simulation modes. Rounded edge (radiused) washers are loaded into the lattice where the present diagnostic box upstream of the IBM gap is located. A maximum of ~22 cm can be accommodated for the Einzel lenses without extending the length of the beam line. A wide variety of Einzel lens geometries can be configured in terms of washer spacing and thickness and polarity of biases (unipolar, bipolar). A field solution for an optimized unipolar Einzel lens with two biased washers is shown in Fig. 5.4. The bias can be varied in time through the use of either user input functions or data files. The data function capability will allow for detailed evaluation of pulsers that will be developed to drive the Einzel lens. This unipolar Einzel lens configuration is considered attractive in spite of the lesser efficiency relative to optimized bipolar structures because it can impart required angular deviations on the beam envelope with an ~80 kV pulse using only a single polarity and easily fit (18 cm length) in the available axial space without lattice extensions.

Figure 5.4: Optimized unipolar Einzel lens geometry with radiused washers imported into the WARP code with upstream (solenoid) and downstream (IBM) lattice structures. Potential contours are superimposed (left) and the on-axis (r=0) potential is shown (right).
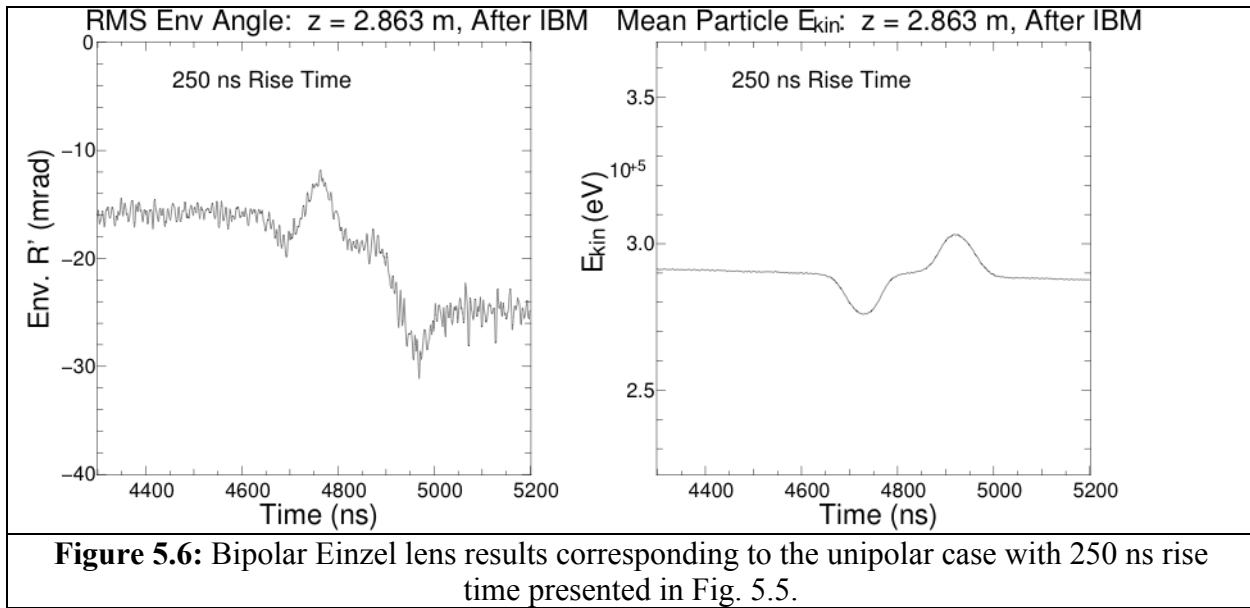
The Einzel lens geometry shown in Fig. 5.4 employs an $r_p = 3$ cm aperture radius which is found to be adequate to minimize beam scraping with a properly tuned beam entering the IBM/neutralization region for drift compression. Washers are separated by $l = 4.5$ cm, which is close enough to optimal spacing to provide sufficient focusing for the desired maximum envelope angle variations at about 80 kV bias while allowing the resulting 18-cm long structure to easily fit in the 22 cm of axial lattice space available. A plate thickness of 15 mm is selected with half-circle radiused edges to hold peak field intensities to about 68 kV/cm (@ 80 kV bias) near the outer edge of the biased plates where the peak field stress region occurs.

Techniques were developed in the code to tune the Einzel lens pulses that required extending the existing code diagnostics. Axisymmetric (*r-z*) simulations were carried out to first optimize the pulses accumulated at fixed *z*-locations in the lattice show that the full transverse focusing effect of the IBM manifests about one pipe radius (fringe length scale) downstream of the gap. Likewise, the full focusing effect of the time variation on the Einzel lens manifests itself only

after the fringe downstream of the Einzel lens. With these features in mind, *r-z* simulations with a static neutralizing plasma are carried out to plot the time variation of the angle of the *rms* beam edge, R', and mean particle kinetic energy, E_{kin}, at a *z*-location one fringe length downstream of the IBM in Fig. 5.5. These plots are generated with the IBM waveform off and a linear ramp Einzel lens waveform timed such that it would be coincident with the time variation induced by the IBM (if turned on) at the *z*-location. The linear ramp Einzel lens pulse turns on at $t = 4450$ ns and has a rises from $V = 0$ to $V = 80$ kV over 250 ns. These plots show the influence of transit time effects associated with the variation of the Einzel lens waveform as the beam particles transit the structure. The transit time effect results in relative acceleration/deceleration of parts of the bunch as evident by the variation of the mean particle kinetic energy E_{kin} in Fig. 5.5 superimposed on the gradual droop from the Marx injector waveform. This transit-time variation can complicate the optical effect of the lens and should be reduced to the extent possible to enable simple Einzel lens correction waveform synthesis. Each biased cell (two washer length spacings) take approximately 75 ns for a particle to transit and as the potential varies significantly over this period, transit time variations in beam energy will become enhanced.

Figure 5.5: Statistical *rms* edge radius R' and particle kinetic energy E_{kin} versus time *t* for a linear ramp Einzel lens waveform induced at a *z*-location one fringe length downstream of the IBM gap. Shown for 250 ns (upper row) and 50 ns (lower row) rise times.
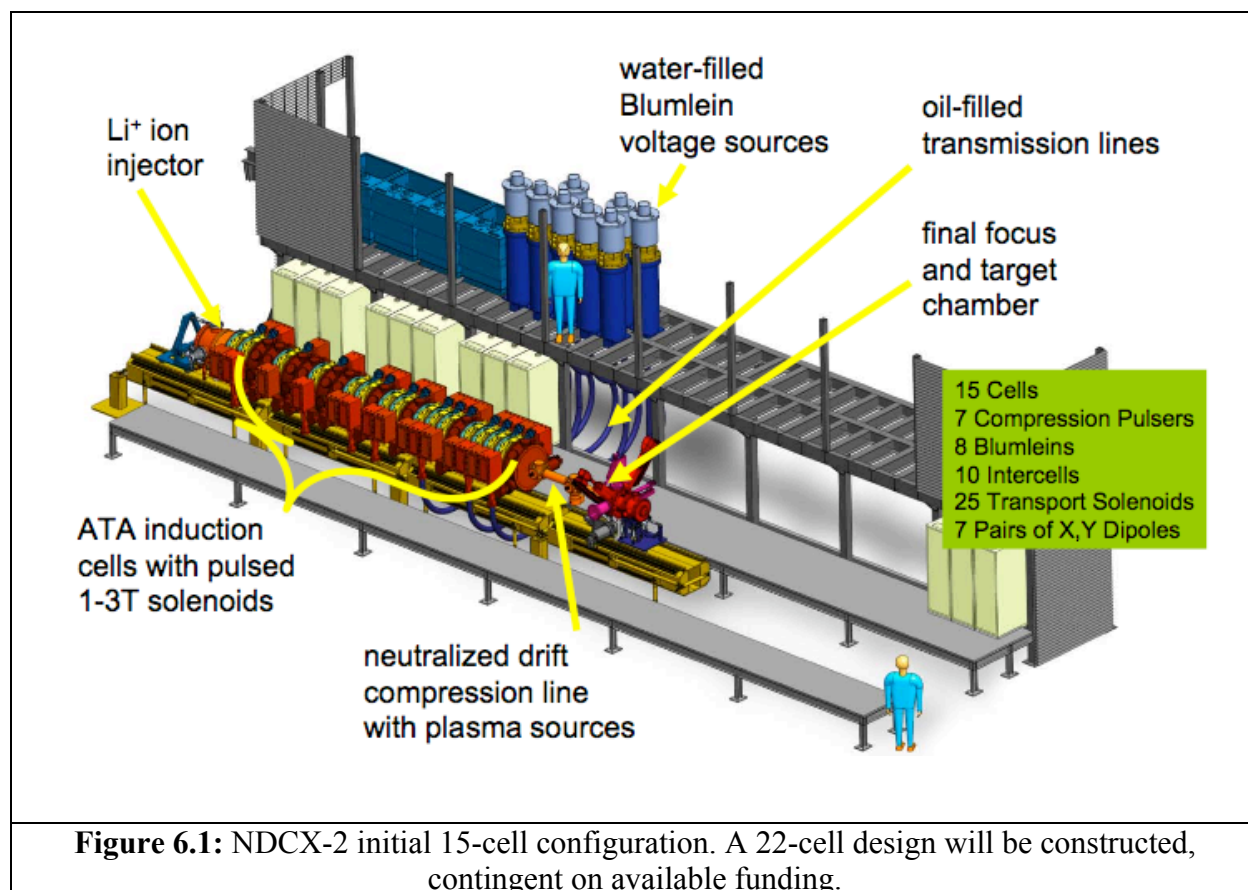
Methods are being explored to compensate for and reduce the complication of this transit time effect. For example, using bipolar structures with an even number of biased plates, or alternatively, shorter plate spacing (*l*) reduces the effect significantly. The increased focusing strength of bipolar relative to unipolar structures allows this choice while still meeting the axial space restrictions for minimal lattice reconfiguration. Peak field stresses for unipolar and bipolar Einzel lens systems with the same plate geometry are almost identical since the peak field stress occurs at the outer edges of the biased plates. So no changes in geometry to mitigate breakdown concerns are required for bipolar operation. Fig. 5.6 shows the case corresponding to Fig. 5.5 with a bipolar Einzel lens formed from the same geometry as the unipolar Einzel lens system with a bipolar bias (first biased washer +*V* and 2nd biased washer -*V*).

Figure 5.6: Bipolar Einzel lens results corresponding to the unipolar case with 250 ns rise time presented in Fig. 5.5.

6. Scaling Considerations for Implementation on NDCX-2

Chromatic aberrations will play a similar role in limiting the peak intensity on target in the NDCX-2. Thus many of the concepts of the Einzel lens approach to the NDCX-1 time-dependent correction can be applied to NDCX-2. In this section we describe differences that lead to interesting challenges on NDCX-2.

Figure 6.1: NDCX-2 initial 15-cell configuration. A 22-cell design will be constructed, contingent on available funding.

NDCX-2 will significantly increase the energy on target, which will allow exploration of warm dense matter conditions that have not been available elsewhere. The NDCX-2 induction linear accelerator (linac) will produce ns-duration ion beam bunches to hit thin foil targets. For lithium ions, kinetic energy in the range $1.5 < E < 5$ MeV have ion deposition ranges that are near the maximum of $dE/dx(E)$. The expected beam charge in the 1 ns (or shorter) pulse is 20 nC or more. The pulse repetition rate will be 1-2/min. A Li^+ beam will be accelerated in an induction accelerator through at least 15 induction cells up to the final ion kinetic energy, and then will be injected into a several meter long drift compression and final focusing channel (See Figs. 6.1 and 6.2).

Figure 6.2: The NDCX-2 22-cell configuration.
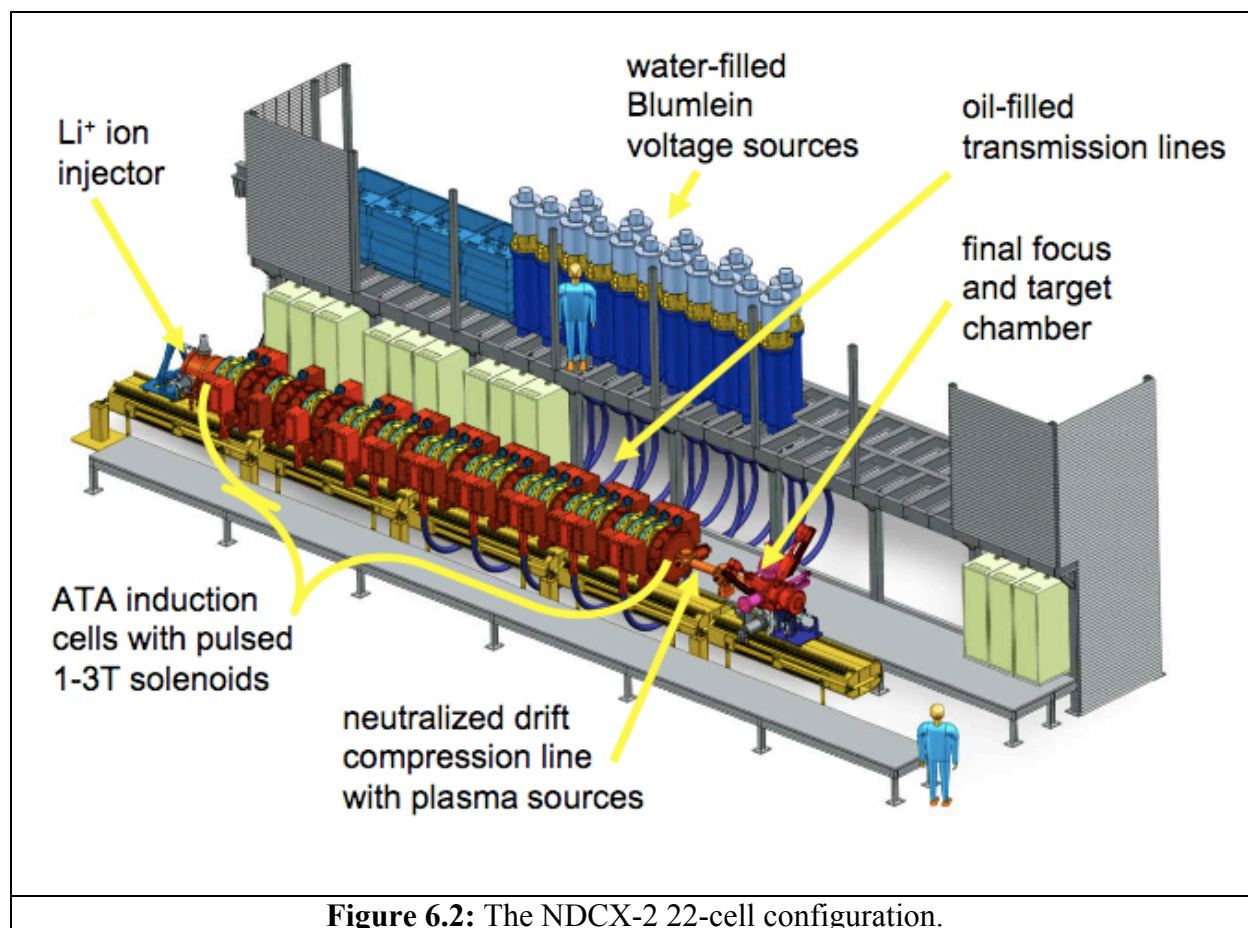
The beam will have a head-to-tail velocity ramp to create the short bunch at the target plane. Transverse focusing will be imparted by a high-field final focus solenoid similar to NDCX-1. Thus the final beam manipulations (ion beam with a velocity ramp, neutralizing plasma, final focusing solenoid) are qualitatively similar to NDCX-1. A comparison of NDCX-1 and NDCX-2 beam parameters is summarized in Table 6.1.

Table 6.1: Beam parameters for NDCX1 and NDCX2. I_{DC} and t_{DC} refer to the beam current and bunch duration at the entrance to the neutralized drift compression section.
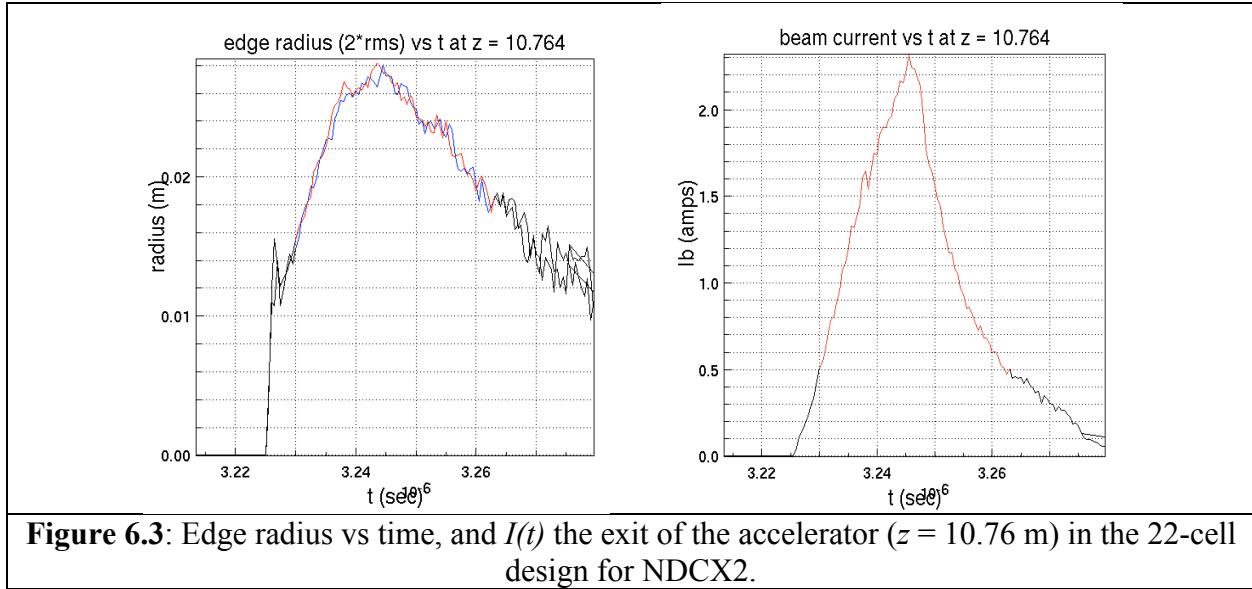
	NDCX1	NDCX2
Ion mass [amu]	39	7
E_{beam} **(min) [MeV]**	0.27	1.5
E_{beam} **(typ) [MeV]**	0.3	3.5
E_{beam} **(max)**	0.35	5
β (min)	3.9E-03	2.1E-02
β (typ)	4.1E-03	3.3E-02
β (max)	4.4E-03	3.9E-02
v_{ion} **(typ) [m/s]**	1.2E+06	9.8E+06
ΔE_{beam} **[keV]**	80	225
ΔE_{beam} / E_{beam} **[%]**	27	6
$I_{DC\,(typ)}$ **[A]**	0.03	2
$t_{DC\,(typ)}$	200-400	25
t_{tgt} **FWHM [ns]**	2-3	1

The most significant differences are that the duration of the beam pulse at the entrance to the neutralized drift compression section is tenfold shorter and that the ion kinetic energy is tenfold greater in NDCX-2. The time-dependent Einzel lens correctors could be located at the exit of the accelerator, or further upstream where the bunch duration is longer.

First, consider locating the chromatic correction system near the entrance to the neutralization channel where the parameters I_{DC} and t_{DC} in Table 6.1 are relevant: The bunch duration is ≈30 ns. Though the fractional energy ramp, ($\Delta E_{beam}/E_{beam}$) is smaller in NDCX-2, the magnitude of the swing is greater (ΔE_{beam} = 225 kV). Thus the characteristic Einzel lens voltage slope, or *dV(t)/dt* of the correction system are significantly greater in NDCX-1.

Due to the much shorter t_{DC} in NDCX-2, transit time effects through an Einzel lens in NDCX-2 are expected to be more pronounced. This may be further exacerbated by the stronger focusing requirements for correcting the higher energy beam leading to the need for large bias voltages or many cell (axially long) structures possibly combined with solenoid focusing. The needed transverse aperture size for the beam will likely prevent using closely spaced washers in Einzel lens structures to reduce transit time effects due to the need to maintain the design lattice spacing (see Sec. 4). Further simulations will clarify these issues.

WARP simulations of NDCX-2 beam propagation reveal a significant variation of the beam envelope over the bunch duration. Fig. 6.3 shows the variation of the beam radius and current vs. time at the exit of the last acceleration and bunching module. Both the current and beam radius vary significantly in contrast to NDCX-1, where the current and radius are nearly constant. This places different constraints on the correction system waveform. Further modeling is underway to evaluate the implications of these differences on the design of the correction system.

Figure 6.3: Edge radius vs time, and *I(t)* the exit of the accelerator (*z* = 10.76 m) in the 22-cell design for NDCX2.

Another possible location for the chromatic correction elements is upstream within the accelerator where the bunch duration is longer. Fig. 6.4 shows that the main bunch duration is 0.3 μs, with a 0.15-μs flat-top in current. This mitigates the challenges caused by the relatively short bunch length at the end of the accelerator, but may make time-dependent correction to the waveform more complicated to calculate due to the significant separation (8 meters and 18 acceleration stations) between correction elements and the exit of the accelerator. Einzel lenses could fit into gaps that are not acceleration stations. This might require a specially designed solenoid and Einzel lens combination to fit into the lattice period of the accelerator (0.3 m). High-resolution diagnostics will be essential. To enable tuning the chromatic corrections within a reasonable amount of time, the diagnostics must be capable of quickly measuring both the envelope parameters R(t) and R'(t) before and after the correction elements and also at the exit of the accelerator before the drift compression section.

Figure 6.4: *I(t)* at *z* = 2.68 m, and a particle plot (*r-z*) in a 22-cell design for NDCX2.
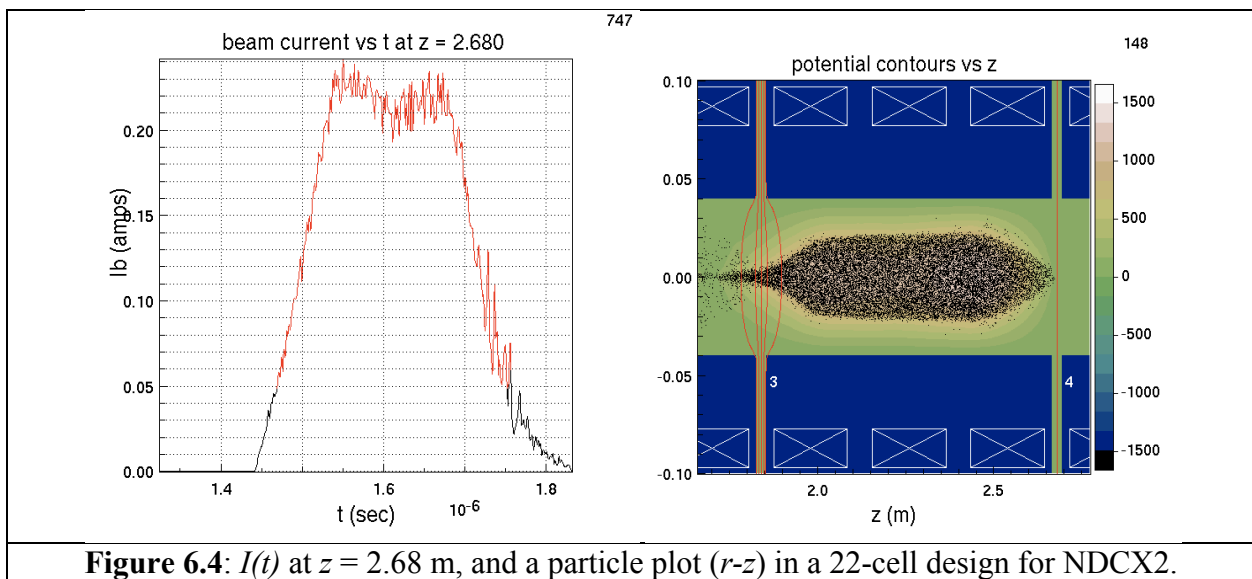
7. Summary and Conclusions

Focal spot differences at the target plane between the compressed and uncompressed regions of the beam pulse have been modeled and measured on NDCX-1. Time-dependent focusing and energy sweep from the induction bunching module are seen to increase the compressed pulse spot size at the target plane by factors of two or more, with corresponding scaled reduction in the peak intensity and fluence on target. A time-varying beam envelope correction lens has been modeled to remove the time-varying aberration.

An Einzel (axisymmetric electrostatic) lens system has been analyzed and optimized for general transport lines, and as a candidate correction element for NDCX-1. Attainable hold-off voltages and temporal variations of the lens driving waveform are seen to effect significant changes on the beam envelope angle over the duration of interest, thus motivating an experimental test on NDCX-1.

Modeling of the beam dynamics in NDCX-1 was performed using a time-dependent (slice) envelope code and with the 3-D, self-consistent, particle-in-cell code WARP. Proof of concept was established with the slice envelope model such that the spread in beam waist positions relative to the target plane can be minimized with a carefully designed Einzel lens waveform and transport line. WARP simulations have verified the behavior of the Einzel lens simulations with a much larger physics effects calculation platform. WARP simulations have also indicated some unpredicted transit time effects, and methods are currently being explored to compensate and reduce this complication. We are proceeding with high resolution modeling and engineering design work to implement an Einzel lens correcting element and the associated high voltage power supplies and pulsers on the NDCX-1 beamline in 2010.

We have explored the use of an Einzel lens, or system of Einzel lenses, to compensate for chromatic aberrations in the beam focal spot in the NDCX-2 target plane. The final beam manipulations in NDCX-2 (linear velocity ramp, charge neutralization, high field final focus solenoid) are similar to NDCX-1 even though the NDCX-2 beam has much higher energy and current. The most relevant distinction though is the pulse duration at the entrance to the drift compression section is tenfold shorter, and the beam energy tenfold higher, than in NDCX-1. Placing a time-dependent, envelope angle correcting element at the neutralized drift region entrance presents a very significant challenge to voltage holdoff and voltage swing in a single Einzel lens. Placing the Einzel lens(es) further upstream reduces the required voltage to effect the necessary envelope correction, while increasing the duration over which the time-dependent voltage must vary. While this simplifies the technological challenge of designing and operating an Einzel lens in NDCX-2, it does require much finer control of the correcting waveform and measurements of its effect on space-charge dominated beams. Additional effort on start-to-end simulations in NDCX-2 using the WARP platform and also with simpler physics models will provide additional clarification on the question of whether a correlated envelope correction can be transmitted downstream against the effects of plasma wave oscillations and beam mixing likely to be present.

---

[i] *MATLAB®* is a product of The Mathworks, Inc.